Article

Gated Photoreactivity of Pyrene Copolymers in Multiresponsive Cross-Linked starPEG-Hydrogels

Dustin Rasch and Robert Göstl*

Cite This: *ACS Polym. Au* 2021, 1, 59−66

Read Online

ACCESS | Metrics & More | Article Recommendations | Supporting Information

ABSTRACT: The synthesis and manufacturing of multiresponsive polymer hydrogels using simple components is a notable challenge. Pyrene is an excimer-forming fluorophore mostly used as microenvironmental probe and for the localization of molecules in close proximity in artificial and biomaterials. Here we make use of the solvophobic preaggregation and photolysis properties of pyrene to construct multiresponsive hydrogels. We synthesize poly(ethylene glycol) (PEG) hydrogels from well-defined pyrene-substituted macro-cross-linkers and elucidate their intricate intra- and intermolecular excimer formation pathways. We find that controlling the water content of the hydrogels through the degree of swelling acts as a gating stimulus governing the photoinduced solvolysis of pyrenylmethyl esters from their poly(methacrylate) backbone. This allows the implementation of a simple transient photolithography process. We thus demonstrate that multiresponsive soft materials with complex optical and mechanical responses can be obtained with comparatively little synthetic effort.

KEYWORDS: hydrogels, pyrene, excimers, lithography, starPEG, photochemistry
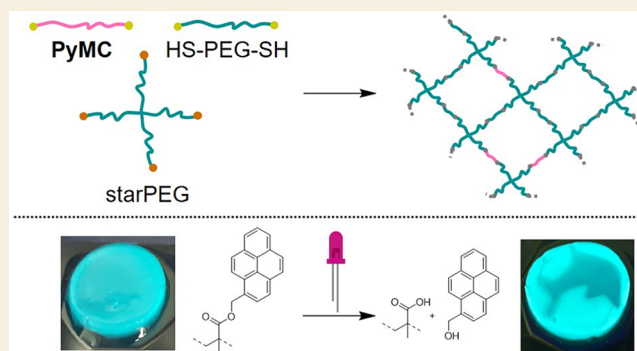
1. INTRODUCTION

Pyrene is one of the most well-characterized fluorophores[1] that forms excimers (excited dimers) at high concentrations and has been investigated ever since the excimer concept was described by Förster.[2] Over the years, the ability to form excimers was discovered in other compounds, *e.g.*, benzene,[3] naphthalene,[4] anthracene,[5] perylene,[6] or 2,5-diphenyloxazole,[7] to name a few. However, the long lifetime of the excited states,[8] high fluorescence quantum yield,[9] good photostability,[9] and sensitivity of the emission spectrum to its surrounding microenvironment[10] gave pyrene an advantage over other excimer-forming systems. Consequently pyrene was used as probe in many applications ranging from organic electronics[11] over sensors for temperature,[12] pH,[13] pressure,[14] force,[15−17] small molecules,[18] protein conformation,[19] lipid structure,[20] or nucleic acid recognition.[21]

Most of these applications make use of the alteration of the ratio between pyrene monomer and excimer emission,[2] which is dependent on the spatial proximity of the pyrene units. However, the extent of excimer formation is influenced by many different parameters, which may even lead to the formation of preassociated, static dimers (and thus excimers) in water due to solvophobic phase segregation.[22] This renders the use of pyrene as distance sensor nontrivial[23] but concomitantly opens up the possibility to exploit such effects for the realization of tailored responsivity in materials.

Here we combine several properties of pyrene to construct hydrogels in which the presence of excimers is controlled photochemically by light.[24,25] In addition, we show that this photoreactivity is gated by the water content of the hydrogels. We apply the combination of these effects in a prototypical hydrogel photolithography process and modulate the mechanical properties of the hydrogels. Importantly, the multiresponsivity of the hydrogels is based solely on the *in situ* manipulation of the tendency of pyrene to form excimers and requires no further auxiliaries, thus rendering the material synthesis very straightforward.

Therefore, we synthesized a series of well-defined statistical copolymers composed of pyrenylmethyl methacrylate (PyMA) and oligo(ethylene glycol) methyl ether methacrylate (OEG-MEMA) with varying pyrene molar proportions χ_{pyrene} by reversible addition−fragmentation chain-transfer (RAFT)[26] polymerization starting from the bifunctional chain-transfer agent (CTA)[27] **2** (Scheme 1a and Table 1). By chemical modification of the end-groups, these were incorporated as covalent macro-cross-linkers **PyMC** into starPEG[28−32] hydro-

Scheme 1. (a) Synthesis of Bifunctional RAFT CTA 2 and from This Poly(PyMA-*co*-OEGMEMA) Macro-Cross-Linkers PyMC and (b) Preparation of starPEG Hydrogels Using PyMC and HS-PEG-SH as Macro-Cross-Linkers
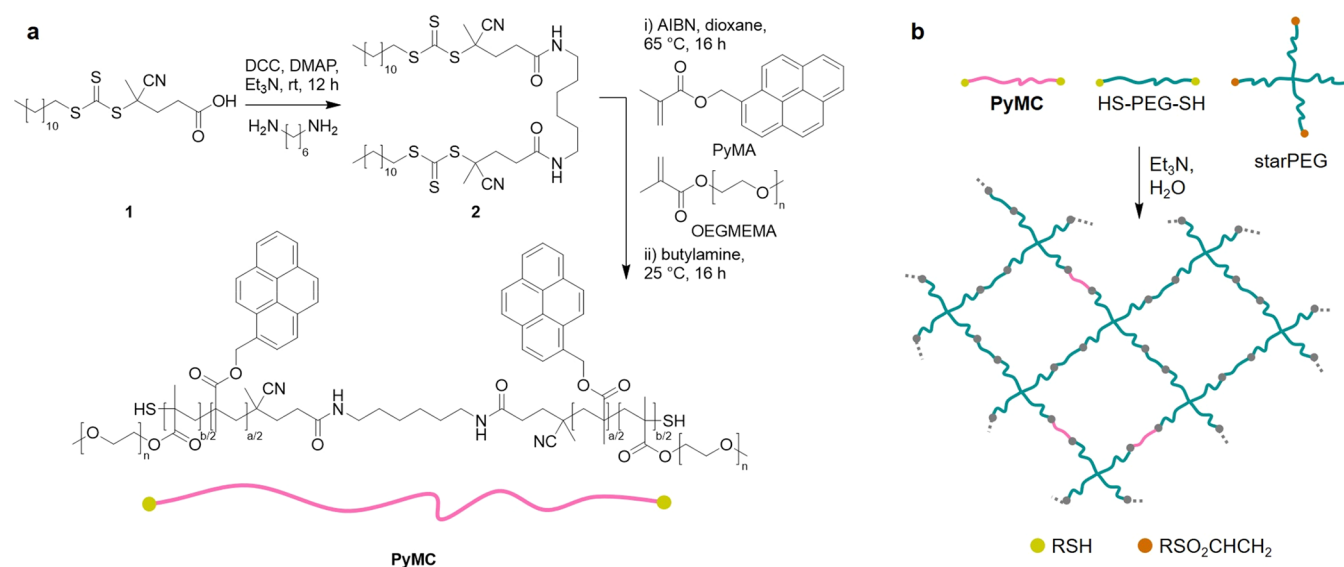
Table 1. Molecular and Spectroscopic Characteristics[a] of Macro-Cross-Linker Copolymers PyMC Synthesized and Investigated in This Work

sample	M_n (g·mol^{-1})[b]	$Đ_M$[b]	X_n $(a + b)$[c]	χ_{pyrene} (mol %)[c]	P_a in H_2O[d]
PyMC$_{24}$	16 830	1.19	53 (13 + 40)	24.4	1.46
PyMC$_{20}$	15 500	1.18	49 (10 + 39)	19.7	1.47
PyMC$_{17}$	20 800	1.20	66 (11 + 55)	17.2	1.43
PyMC$_{14}$	15 300	1.20	48 (7 + 41)	14.5	1.56
PyMC$_{11}$	16 400	1.20	52 (6 + 46)	11.4	1.54
PyMC$_{10}$	18 300	1.25	58 (6 + 52)	10.5	1.64; 2.30[e]
PyMC$_{09}$	19 300	1.20	61 (6 + 55)	9.5	1.69
PyMC$_{08}$	23 000	1.20	74 (6 + 68)	8.0	1.64
PyMC$_{01}$	40 000	1.79	131 (1 + 130)	0.8	2.34

[a]Such as number-average molar mass M_n, molar mass dispersity $Đ_M$, number-average degree of polymerization X_n (including incorporated PyMA a and OEGMEMA b, Scheme 1a), pyrene molar proportion χ_{pyrene}, and peak-to-valley ratio P_a of the (0,0) transition. [b]Determined by GPC. [c]Determined by ^{1}H NMR. [d]Calculated from the UV−vis absorption spectra. [e]In THF.

gels (Scheme 1b). The emissive properties of the hydrogels were strongly dominated by intra- and intermolecular effects depending on intrachain χ_{pyrene} and the overall pyrene mass concentration ρ_{pyrene}. We show that static excimer emission from preassociated pyrene aggregates, which we clearly distinguish from dynamic pyrene excimer emission, is a major contributor to the observed effects.

2. EXPERIMENTAL SECTION

Materials

PyMA was synthesized after a literature protocol.[33] Et$_3$N (99.5%, dry), 4-(dimethylamino)pyridine (99%, DMAP), 1,6-diaminohexane (98%), OEGMEMA (M_n = 300), and 2,2′-azobis(2-isobutyronitrile) (98%, AIBN) were obtained from Merck. OEGMEMA was filtered over basic Al$_2$O$_3$, and AIBN was recrystallized from hexane before use. CH$_2$Cl$_2$ (99.9%, dry) and DMF (99.8%) were obtained from Acros Organics. EtOH (99.8%) was purchased from Fisher Scientific. 4-Cyano-4-[(dodecylsulfanylthiocarbonyl)sulfanyl]pentanoic acid (1) (97%), N-ethyl-N'-(3-(dimethylamino)propyl)carbodiimide hydrochloride (98%, EDC·HCl), and tris(2-carboxylethyl)phosphine hydrochloride (99%, TCEP) were bought from abcr. Dialysis membranes were bought from Spectrum Laboratories (MWCO: 1 kDa). SH-PEG-SH (M_n = 2 kDa, X_n = 45, 99%) and 4-arm

vinylsulfone-terminated starPEG (M_n = 10 kDa, 99%) were obtained from Creative PEGworks.

Methods

NMR spectra were recorded at room temperature in CDCl$_3$ on a 400 MHz Bruker Avance 400 (^{13}C: 101 MHz). Chemical shifts were reported in δ units using residual protonated solvent signals as internal standard. FTIR spectra were recorded in ATR-mode on a Thermo Nicolet Nexus 470. Molar masses (M_n and M_w) and dispersities ($Đ_M$) were determined by gel permeation chromatography (GPC). GPC was performed using tetrahydrofuran (THF) (≥99.7%, unstabilized, HPLC grade, VWR) as eluent. The machine was equipped with an HPLC pump (1260 Infinity II, Agilent) and refractive index (RI) (1290 Infinity II, Agilent), UV (UV-2075plus, Jasco), and multiangle light scattering (MALS) (SLD 7100, Polymer Standards Service) detectors. The samples contained 250 mg·mL^{-1} 3,5-di-*tert*-4-butylhydroxytoluene (BHT, ≥ 99%, Fluka) as the internal standard. One precolumn (8 × 50 mm) and four SDplus gel columns (8 × 300 mm, MZ Analysentechnik) were used at a flow rate of 1.0 mL·min^{-1} at 20 °C. The diameter of the gel particles was 5 μm, and the nominal pore widths were 50, 10^2, 10^3, and 10^4 Å. Calibration was performed using narrow-disperse poly(methyl methacrylate) standards (Polymer Standards Service). Results were evaluated using the PSS WinGPC UniChrom software (version 8.3.2). Rheometry was performed on a Discovery HR-3 from TA Instruments. A 20 mm parallel Peltier steel plate was used. For *in*

situ UV irradiation, an LED (λ_{max} = 365 nm, I = 3 mW·cm^{-2}) was fiber-coupled into the system by a collimator setup and uniformly covered the whole sample. Data evaluation was performed with Trios Software (ver. 4.4.0.41128).

Bifunctional CTA 2 for RAFT

2 was synthesized by a Steglich amidation. DMAP (0.48 g, 3.9 mmol), EDC·HCl (0.74 g, 3.9 mmol), 1,6-diaminohexane (0.17 g, 1.5 mmol), and Et$_3$N (0.70 g, 6.9 mmol) were dissolved in dry CH$_2$Cl$_2$ (18 mL) and few drops of dry DMF and the solution was cooled to 0 °C. Then, **1** (1.2 g, 3 mmol) in dry CH$_2$Cl$_2$ (6 mL) was added slowly and the whole stirred at room temperature overnight. The mixture was then diluted with CH$_2$Cl$_2$ and washed with saturated aqueous NH$_4$Cl, Na$_2$CO$_3$, and NaCl solutions. The organic layer was dried over MgSO$_4$ and the solvent evaporated *in vacuo*. The product was purified by silica column chromatography with heptane and EtOAc (1:2, R_f = 0.22) yielding a yellow solid (22%). ^{1}H NMR (CDCl$_3$), δ (ppm): 5.74 (s, 2H, NHCO), 3.36−3.17 (m, 8H), 2.62−2.28 (m, 8H), 1.95−1.00 (m, 48H), 0.86 (t, 6H, CH$_3$). See Figure S4. FTIR ν (cm^{-1}): 3264 (amide A), 3087 (amide B), 2232 (CN), 1634 (amide 1), 1584 (amide 2). See Figure S7. The synthesis of monofunctional CTA **3** for the synthesis of control polymer **PyMC$_{01}$** is described in the Supporting Information.

Synthesis of PyMC

CTA **2** (1 equiv) was used in statistical copolymerizations of PyMA (*n* equiv) and OEGMEMA (70 − *n* equiv) in dry 1,4-dioxane (66 wt %). To this, AIBN (0.1 equiv) was added, and the solution was heated at 65 °C for 18 h achieving conversions >90%. The obtained polymers were dialyzed against THF and then against H$_2$O. The polymers were analyzed by GPC and ^{1}H NMR (Figures S9−S26). The feed ratio for PyMA during polymerization was slightly higher than the incorporated ratio that was found in **PyMC** (*a* and *b* in Table 1) by ^{1}H NMR. Hereafter, the terminal trithiocarbonates were aminolyzed by the addition of *n*-butylamine (30 equiv) under Schlenk conditions in THF (0.012 mol·L^{-1}) in the presence of TCEP. Hereafter, the polymer was dialyzed against THF and then H$_2$O, dried *in vacuo*, and colorless **PyMC** (Table 1) were received. The end group fidelity of the generated terminal thiols was estimated by using Ellman's reagent.[34] For the synthesis of control polymer **PyMC$_{01}$**, CTA **3** was used in a homopolymerization of OEGMEMA (200 equiv) under otherwise identical conditions. Dye-induced aggregation of the CTA possibly was the reason for the high $Đ_M$.

Preparation of the Hydrogels

This was performed by step-growth polymerization of **PyMC** macro-cross-linkers (*z* equiv) alongside HS-PEG-SH (2 − *z* equiv) and 4-arm starPEG terminally functionalized with 4× vinyl sulfone (1 equiv) via a thiol−ene reaction at pH = 8−10. As an example, starPEG (2.1 µmol, 20.7 mg), HS-PEG-SH (3.9 µmol, 7.9 mg), and **PyMC$_{17}$** (0.2 µmol, 3.4 mg) were dissolved in H$_2$O (200 µL) and cast into a PTFE-coated metal mold. After the addition of Et$_3$N (30 µL), the mold was covered and left to react overnight. The hydrogels were immersed in H$_2$O to remove residual reactants yielding transparent hydrogels with visible blue or green fluorescence based on the identity and fraction of incorporated **PyMC**.

Optical Experiments

UV−vis absorption spectroscopy was performed on a Thermo Scientific Evolution 300 and fluorescence spectroscopy on a Horiba Fluoromax-4P at room temperature in H$_2$O (VWR, HPLC grade) and THF (VWR, Reag. Ph Eur). Excitation and emission spectra of the hydrogels were recorded with a compact spectrometer (CCS200, Thorlabs). A fiber-coupled LED (M340F3, Thorlabs) was used as a light source. The emission was detected simultaneous to the excitation with a fiber Y-bundle reflection probe (RP24, Thorlabs), which also transmitted the excitation light. The spectra were analyzed with the Thorlabs OSA software (version 2.90).

3. CHARACTERIZATION OF PYRENE MACRO-CROSS-LINKERS

Before any spectroscopic analyses of the **PyMC** macro-cross-linkers or their incorporation into hydrogels were performed, we verified their solubility in water. While all **PyMC** derivatives were soluble at room temperature, some variants showed critical solution temperatures (CSTs). For example, **PyMC$_{24}$** as the most hydrophobic derivative showed a cloud point temperature T_{CP} of 33 °C (Figure S1). The CSTs were overall only mildly dependent on polymer mass concentrations ρ_{PyMC}, but they were influenced significantly by increasing pyrene molar proportions χ_{pyrene} within the chain that, expectedly, led to lower T_{CP}.[35]

PyMC derivatives at constant ρ_{PyMC} were then investigated by fluorescence spectroscopy (Figure 1a). From control
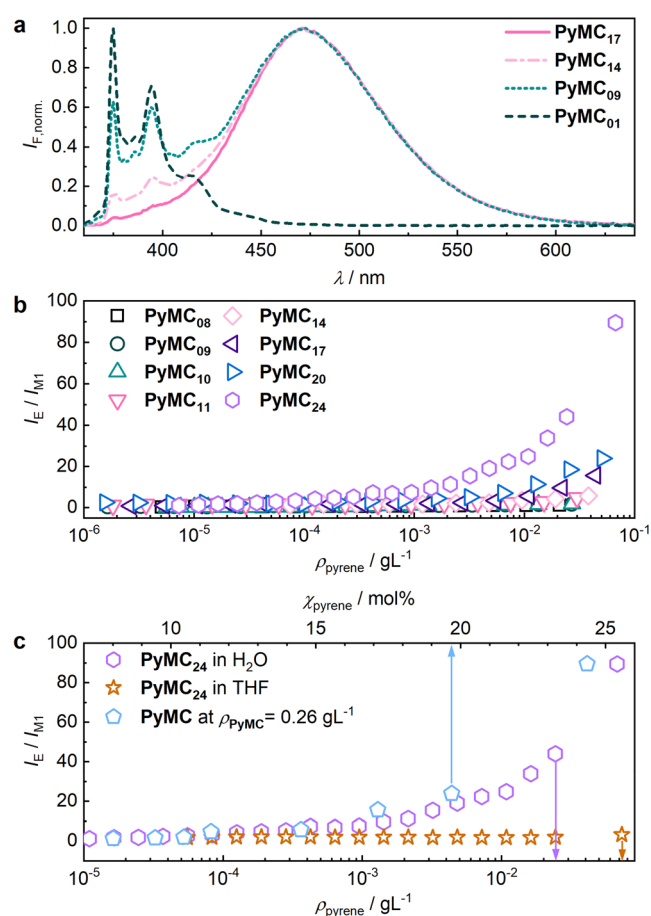
Figure 1. Pyrene emission in dependence of different **PyMC** concentrations. (a) Normalized (to maximum) emission spectra of four **PyMC** derivatives with varying χ_{pyrene} (Table 1) at ρ_{PyMC} = 0.26 g·L^{-1} and λ_{exc} = 340 nm. (b) Excimer to monomer emission ratio I_E/I_{M1} as a function of the solution pyrene mass concentration ρ_{pyrene}. (C) I_E/I_{M1} as a function of ρ_{pyrene} for **PyMC$_{24}$** in THF or H$_2$O (bottom *x*-axis) as well as a function of the intrachain pyrene molar proportion χ_{pyrene} of **PyMC** derivatives at constant ρ_{PyMC} (top *x*-axis).

polymer **PyMC$_{01}$**, bearing exactly one pyrene unit per chain, to **PyMC$_{17}$**, it became clear that an increasing intrachain χ_{pyrene} led to an increased excimer emission progressively repressing the role of monomer emission. While the latter was mostly characterized through two narrow peaks at 375 and 395 nm

(band 1 and 3, respectively), the former was observed as mostly broad, featureless peak between 425 and 630 nm.

Complete emission spectra were then reduced to the ratio of the emission intensities of excimer I_E at 475 nm and of monomer band 1 I_{M1} at 375 nm. In addition to intrachain χ_{pyrene}, this reduction then allowed us to assess the role of increasing pyrene solution mass concentration ρ_{pyrene} by plotting the I_E/I_{M1} ratio as a function of ρ_{pyrene} for all **PyMC** derivatives (Figure 1b). Toward infinite dilution, all macro-cross-linkers exhibited a comparably low I_E/I_{M1} ratio, while at increasing ρ_{pyrene}, those derivatives with high χ_{pyrene} exhibited disproportionately high excimer emission. This trend was visualized even more clearly by plotting the I_E/I_{M1} ratio directly as a function of χ_{pyrene} for all macro-cross-linkers at constant ρ_{PyMC} (Figure 1c, top axis). These observations suggested that either interchain excimer formation dominated over intrachain excimer formation or that interchain hydrodynamic compression due to passing the overlap concentration gained importance at concentrations relevant for spectroscopic measurements in materials.

Notably, excimer emission of the macro-cross-linkers showed a strong solvent dependence. For example, while the I_E/I_{M1} ratio of **PyMC$_{24}$** increased dramatically with increasing ρ_{pyrene} in H_2O, only a very mild increase was observed in THF (Figure 1c, bottom axis). Since the formation of interchain excimers was hence suppressed by certain solvents, we hypothesized that excimer formation in our system was not dominated by the usually observed dynamic mechanism[36] but conversely was rooted in static, e.g., solvophobic, effects. The formation of preassociated pyrene aggregates in water was reported to the literature before and was characterized both by the broadening and bathochromic shift of the absorption spectra and by the peak-to-valley ratio $P_a = A_{peak}/A_{valley}$ between the absorption maximum at ca. 350 nm and its corresponding valley at ca. 338 nm.[22]

We investigated whether the excimers of the macro-cross-linkers exhibited a bathochromic shift by comparing normalized excitation spectra at emission wavelengths indicative of mostly independent monomer (394 nm) and excimer (480 nm) emission. While, representatively, **PyMC$_{10}$** showed a clear bathochromic shift in the excimer compared to the monomer excitation spectrum in water (Figure 2a), no such effect was observed in THF (Figure 2b). In addition, we found that P_a significantly decreased with increasing χ_{pyrene} (Figure 2c, Table 1, and Figures S2 and S3). Both observations strongly suggested the presence of preassociated, static pyrene aggregates that likely formed due to solvophobic effects in H_2O, but not in THF.

We then noticed that the excitation spectra of **PyMC$_{10}$** were dissimilar after measurements in the fluorescence spectrometer (Figure 2d). On the one hand, the excimer emission decreased while the monomer emission increased over 75 min. On the other hand, we observed an increased P_a value after the measurements hinting toward a decrease in static excimer presence. We found that this was caused by the photoinduced solvolysis of the pyrenylmethyl esters by irradiation at 340 nm, which was documented in the literature before for the release of pyrene as small molecule[24] or for the disassembly of micelles.[25]

To investigate the photolysis in more detail, we measured fluorescence spectra under constant excitation of **PyMC$_{17}$** (Figure 3a). Over the course of the irradiation, the initial I_E/I_{M1} ratio of 1.807 rapidly decreased to 0.029 (Figure 3b). This
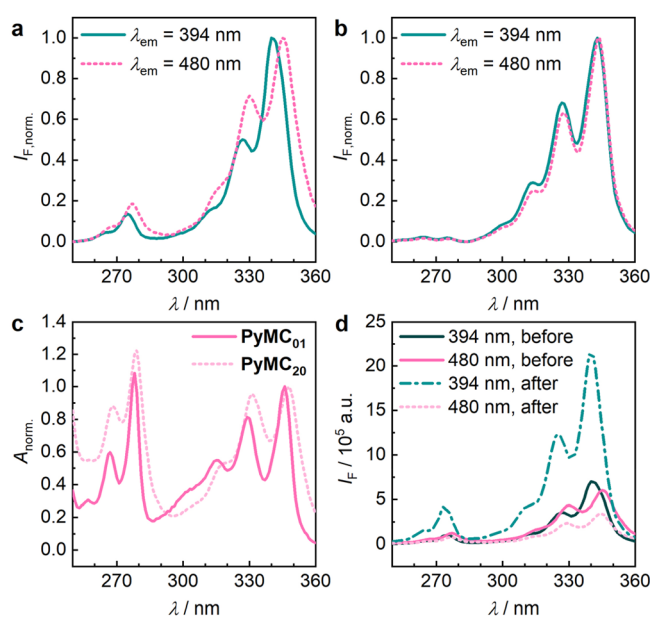

Figure 2. Pyrene aggregation behavior within **PyMC** in dependence of solvent, χ_{pyrene}, and irradiation duration. (a) Normalized (to maximum) excitation spectra of **PyMC$_{10}$** in H_2O with emission measured at the monomer and excimer maximum (ρ_{PyMC} = 0.016 g·L^{-1}). (b) Normalized (to maximum) excitation spectra of **PyMC$_{10}$** in THF with emission measured at the monomer and excimer peak (ρ_{PyMC} = 0.016 g·L^{-1}). (c) Normalized (to (0,0) transition) absorption spectra of **PyMC$_{01}$** and **PyMC$_{20}$** in H_2O (ρ_{PyMC} = 0.033 g·L^{-1}). (d) Excitation spectra of **PyMC$_{10}$** (ρ_{PyMC} = 0.016 g·L^{-1}) in H_2O at the monomer and excimer peak before and after irradiation sustained (75 min, λ_{exc} = 340 nm) during measurements.

was accompanied by a polarity increase of pyrenes' microenvironment as signified by the ratio of the first and third monomer emission peaks I_{M1}/I_{M3},[10] which increased from 1.1 to 1.2. In addition, the fluorescence spectra featured an isostilbic point at 439 nm, suggesting the absence of side reactions.[2] Notably, this photoreaction was not observed in THF once more corroborating the photoinduced solvolysis process as the presence of protic and nucleophilic solvents was required for this mechanism (Figure 3c).[37]

To conclude, we here tuned the intrachain pyrene molar proportion χ_{pyrene} of macro-cross-linkers **PyMC** such that strong static excimer formation in aqueous solution driven by solvophobic pyrene association was observed. These macro-cross-linkers underwent efficient and clean photolysis in H_2O, which led to the release of 1-pyrenemethanol, its migration into free solution, and the disintegration of the static excimers favoring monomer emission. We thus showed that the photoreactivity of pyrenylmethyl esters depended on the identity of the solvent potentially allowing the external gating of this process in gels by solvent exchange.

4. HYDROGELS FROM PYRENE MACRO-CROSS-LINKERS

Hydrogels exhibited an equilibrium degree of swelling d_s larger than 4500%. The solvophobic pyrene association, described for the macro-cross-linkers **PyMC** above, caused a strong dependence of the excimer emission from d_s and was observed through the I_E/I_{M1} emission ratio. For example, a hydrogel containing z = 0.1 equiv of **PyMC$_{17}$** showed an I_E/I_{M1} ratio of ca. 16.5 in the equilibrium-swollen state while in the dry state
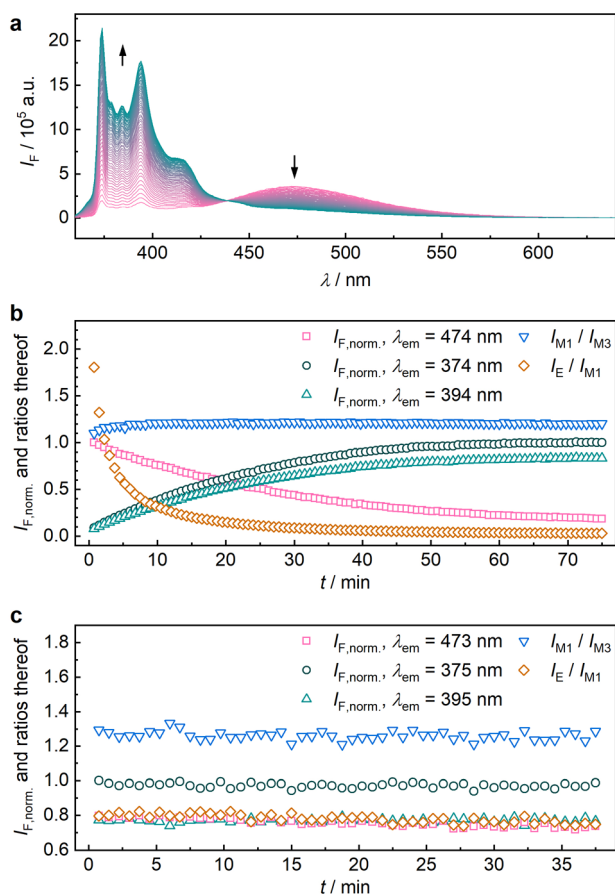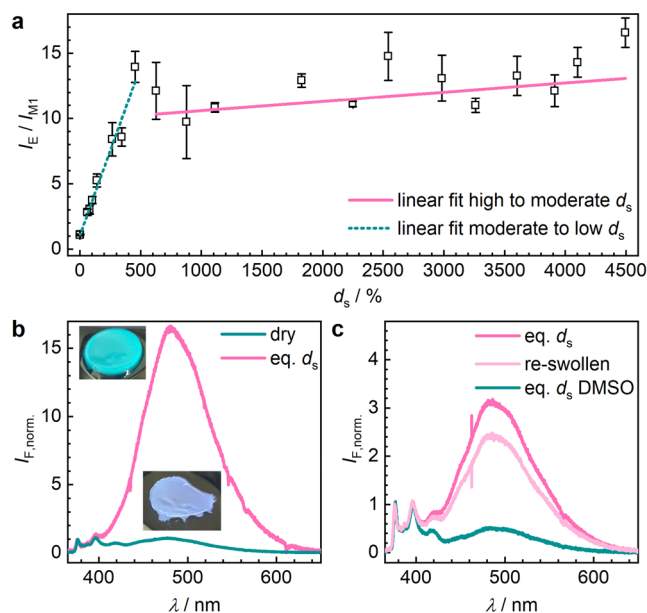
Figure 3. Photolysis of **PyMC$_{17}$** (ρ_{pyrene} = 5.5 × 10^{-4} g·L^{-1}, λ_{exc} = 340 nm) as a function of irradiation time t. (a) Emission spectra from 0 to 75 min irradiation in H$_2$O. (b) Progression of emission maxima from monomer and excimer emission collected from normalized emission spectra including I_{M1}/I_{M3} and I_E/I_{M1} ratios for irradiation in H$_2$O and (c) in THF.

Figure 4. Dependence of pyrene excimer emission from degree of swelling d_s in **PyMC**-cross-linked hydrogels. (a) Excimer to monomer emission ratio I_E/I_{M1} as a function of d_s for **PyMC$_{17}$**-cross-linked (z = 0.1 equiv) hydrogel. Mean values ± SD from the mean. N = 3 individual spectra obtained at different positions of the hydrogel. (b) Normalized (to M1) emission spectra (λ_{exc} = 340 nm) of dry and equilibrium-swollen (ρ_{pyrene} = 0.40 g·L^{-1}) **PyMC$_{17}$**-cross-linked (z = 0.1 equiv) hydrogel including photographs of the gels in their respective state as insets (λ_{exc} = 365 nm). (c) Normalized (to M1) emission spectra (λ_{exc} = 340 nm) of **PyMC$_{08}$**-cross-linked (z = 0.2 equiv) gels: equilibrium-swollen in H$_2$O; dried, then equilibrium reswollen in H$_2$O; and equilibrium-swollen in DMSO.

I_E/I_{M1} was ca. 1.1 (Figure 4, parts a and b). This process was reversible by reswelling (Figure 4c).

Notably, the I_E/I_{M1} ratio varied discontinuously with d_s exhibiting a slight decrease from high to moderate d_s while transforming into a strong decrease from moderate to low d_s. We attributed this observation to the sudden dissolution of the preassociated pyrene into the (comparably more) hydrophobic polymer backbone, once a threshold d_s was surpassed. This phenomenon was discovered recently and in parallel to our own work by Hamasaki and co-workers on pyrene solution-blended into poly(N-isopropylacrylamide) hydrogels.[38] However, in our materials, this effect was considerably more pronounced as the covalent attachment of the pyrene units to the polymer backbone allowed higher pyrene loading preventing its precipitation from aqueous solution at high d_s. Aggregation-caused quenching (ACQ) as origin for these observations[39] was ruled out due to the increase of the monomer emission accompanying the decrease of the excimer emission (Figure S27).

Analogous to the experiments on **PyMC$_{24}$** in THF (Figure 1c), equilibrium-swelling the networks in DMSO also led to a significant decrease of excimer formation, once again underlining the solvophobic preassociation mechanism of excimer formation (Figure 4c). This effect was reversible but showed some fatigue likely stemming from residual water in both the

dried polymer networks and DMSO. Consequently, either drying the hydrogels or swelling them in aprotic solvent thus led to the same dissolution of preassociated pyrene.

We then used this effect to gate the photoreactivity of **PyMC$_{10}$**-cross-linked hydrogels. In the equilibrium swollen state, this hydrogel exhibited an I_E/I_{M1} ratio of 8.45, and expectedly, the irradiation with a conventional 6 W laboratory UV hand lamp at λ_{exc} = 365 nm for 60 min decreased this value to 0.25 as 1-pyrenemethanol was photochemically released into solution (Figure 5, pink). This excimer emission depletion was also not recovering over time, once more underlining the irreversible photoinduced release process. Then, an air-dried hydrogel sample was subjected to the same sequence. While excimer emission was expectedly low with an I_E/I_{M1} ratio of 0.55 in the dry state due to the dissolution of pyrene within the polymer backbone, irradiation conditions identical with those used above led to no significant change in the I_E/I_{M1} ratio (Figure 5, green). Conversely, reswelling the dry and irradiated sample to equilibrium with H$_2$O clearly recovered the strong excimer emission caused by solvophobic pyrene preassociation to I_E/I_{M1} = 4.67. Most notably, this demonstrates how the presence of water as expressed though d_s served as additional gating stimulus to control the photolysis of the pyrenylmethyl esters.

The effects described above in combination with the pronounced excimer emission in **PyMC$_{17}$**-cross-linked hydro-gels, which was visible by the naked eye, allowed us to use this system in a simple prototypical transient photolithography process. By covering parts of the hydrogel with a dolphin-shaped negative photomask and irradiation with a UV hand
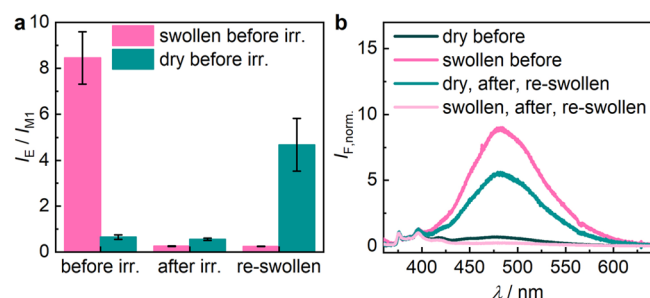
Figure 5. Gating the photoreactivity of **PyMC$_{10}$**-cross-linked ($z = 0.1$ equiv) hydrogels by the degree of swelling d_s exemplified on an equilibrium-swollen hydrogel (pink) and a dry hydrogel (green). (a) Bar graph showing the excimer to monomer emission ratio I_E/I_{M1} for the three states: before irradiation, after irradiation, and upon reswelling after irradiation of the two hydrogel samples. Mean values ± SD from the mean. $N = 3$ individual spectra obtained at different positions of the hydrogels. (b) Normalized (to M1) emission spectra ($\lambda_{exc} = 340$ nm) of the two hydrogel samples of panel a in the two states: before irradiation (dark color) and upon reswelling after irradiation (light color).

lamp at $\lambda_{exc} = 365$ nm for 30 min, only those areas that were exposed to UV light lost their strong green excimer emission (Figure 6a). While the dolphin was immediately visible, the
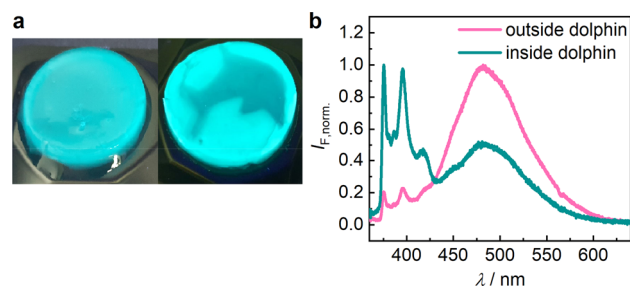
Figure 6. A simple photolithographic process using of **PyMC$_{17}$**-cross-linked ($z = 0.1$ equiv) hydrogels using a dolphin-shaped negative photomask. (a) Hydrogel before (left) and after (right) irradiation with 6 W UV hand lamp at $\lambda_{exc} = 365$ nm for 30 min through the photomask. (b) Normalized (to maximum) emission spectra ($\lambda_{exc} = 340$ nm) of the hydrogel after irradiation taken either outside or inside of the dolphin.

actual emission spectra recorded locally at the respective sites of the sample additionally clearly indicated where irradiation occurred and the results thereof (Figure 6b). Note that the I_E/I_{M1} ratio was slightly lower after the lithography in Figure 6b compared to Figure 4b due to diffracted and reflected light leading to partial photolysis also in the formally nonirradiated region. The developed image was only permanent when it was not actively watched under UV irradiation (up to 30 min), since the observation and writing wavelengths were identical.

In addition, we investigated whether the mechanical properties of the hydrogels were altered by the photolysis process. For this, we placed monomer solutions in a plate rheometer and followed both the formation and subsequent photolysis of **PyMC$_{17}$**-cross-linked hydrogels *in situ* through the observation of the storage (G') and loss modulus (G'') (Figure 7a). Already after 30 min the storage modulus plateaued indicating a mostly finished gelation. Over the course of the subsequent *in situ* irradiation with UV-light a significant increase of G' was observed. Since control
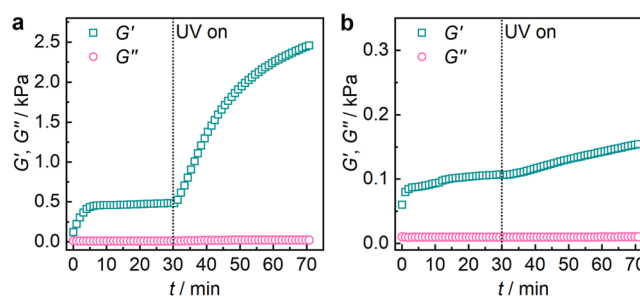
Figure 7. Behavior of the storage (G') and loss modulus (G'') during polymerization and subsequent photolysis of (a) **PyMC$_{17}$**-cross-linked ($z = 0.1$ equiv) hydrogel and b) solely HS−PEG−SH-cross-linked hydrogel. UV irradiation inside the plate rheometer was turned on after 30 min. A strain amplitude of $\gamma_0 = 1\%$ at a frequency of $\omega_1/2\pi = 1$ Hz was used.

experiments using solely HS−PEG−SH cross-linked hydrogels showed no such effect (Figure 7b), we hypothesized that the photolytic dissolution of pyrene aggregates and the associated transformation of the poly(methacrylate) to a poly(methacrylic acid) backbone caused this behavior.

5. CONCLUSIONS

We here demonstrated that the covalent modification of PEG-based hydrogels with pyrene allowed the straightforward manufacturing of multiresponsive materials. We synthesized hydrogels from well-defined pyrene-substituted macro-cross-linkers and elucidated their intra- and intermolecular excimer formation pathways in dependence of intrachain pyrene molar proportion χ_{pyrene} and the overall pyrene mass concentration ρ_{pyrene}. Additionally, we found that the degree of swelling d_s of the hydrogels allowed gating the photoinduced solvolysis of pyrenylmethyl esters from their poly(methacrylate) backbone. The combination of the investigated effects allowed the implementation of a simple transient photolithography process and the variation of the stiffness of these hydrogels. Through the straightforward synthesis and the reliance on the intrinsic photochemical and -physical properties of pyrene alone, we demonstrated that multiresponsive soft materials with complex optical and mechanical responses can be obtained with comparatively little synthetic effort. We hence believe that pyrene-based gated functional transitions could find applications in many soft materials to control complex functionality.

■ ASSOCIATED CONTENT

ⓈI Supporting Information

The Supporting Information is available free of charge at https://pubs.acs.org/doi/10.1021/acspolymersau.1c00011.

> GPC and ^{1}H NMR spectra, calculations for χ_{pyrene}, cloud point measurements, calculation of d_s and P_a, FTIR and ^{1}H NMR spectra of **2**, and the synthesis of CTA **3** (PDF)

■ AUTHOR INFORMATION

Corresponding Author

Robert Göstl − *DWI−Leibniz Institute for Interactive Materials, 52056 Aachen, Germany;* ⦿ orcid.org/0000-0002-7483-6236; Email: goestl@dwi.rwth-aachen.de

Author

Dustin Rasch — *DWI—Leibniz Institute for Interactive Materials, 52056 Aachen, Germany; Institute of Technical and Macromolecular Chemistry, RWTH Aachen University, 52074 Aachen, Germany*

Complete contact information is available at:
https://pubs.acs.org/10.1021/acspolymersau.1c00011

Author Contributions

The manuscript was written through contributions of all authors. All authors have given approval to the final version of the manuscript.

Notes

The authors declare no competing financial interest.

■ REFERENCES

(1) Förster, T.; Kasper, K. Ein Konzentrationsumschlag der Fluoreszenz des Pyrens. *Z. Elektrochem. Ber. Bunsenges. Phys. Chem.* **1955**, *59* (10), 976−980.

(2) Förster, T. Excimers. *Angew. Chem., Int. Ed. Engl.* **1969**, *8* (5), 333−343.

(3) Cardozo, T. M.; Galliez, A. P.; Borges, I.; Plasser, F.; Aquino, A. J. A.; Barbatti, M.; Lischka, H. Dynamics of Benzene Excimer Formation from the Parallel-Displaced Dimer. *Phys. Chem. Chem. Phys.* **2019**, *21* (26), 13916−13924.

(4) Jones, P. F.; Nicol, M. Excimer Emission of Naphthalene, Anthracene, and Phenanthrene Crystals Produced by Very High Pressures. *J. Chem. Phys.* **1968**, *48* (12), 5440−5447.

(5) McVey, J. K.; Shold, D. M.; Yang, N. C. Direct Observation and Characterization of Anthracene Excimer in Solution. *J. Chem. Phys.* **1976**, *65* (8), 3375−3376.

(6) Walker, B.; Port, H.; Wolf, H. C. The Two-Step Excimer Formation in Perylene Crystals. *Chem. Phys.* **1985**, *92* (2), 177−185.

(7) Agbaria, R. A.; Gill, D. Extended 2,5-Diphenyloxazole-.Gamma.-Cyclodextrin Aggregates Emitting 2,5-Diphenyloxazole Excimer Fluorescence. *J. Phys. Chem.* **1988**, *92* (5), 1052−1055.

(8) Birks, J. B.; Dyson, D. J.; Munro, I. H.; Flowers, B. H. 'Excimer' Fluorescence II. Lifetime Studies of Pyrene Solutions. *Proc. R. Soc. London A* **1963**, *275* (1363), 575−588.

(9) de Halleux, V.; Mamdouh, W.; De Feyter, S.; De Schryver, F.; Levin, J.; Geerts, Y. H. Emission Properties of a Highly Fluorescent Pyrene Dye in Solution and in the Liquid State. *J. Photochem. Photobiol., A* **2006**, *178* (2), 251−257.

(10) Dong, D. C.; Winnik, M. A. The Py Scale of Solvent Polarities. *Can. J. Chem.* **1984**, *62* (11), 2560−2565.

(11) Figueira-Duarte, T. M.; Müllen, K. Pyrene-Based Materials for Organic Electronics. *Chem. Rev.* **2011**, *111* (11), 7260−7314.

(12) Pietsch, C.; Vollrath, A.; Hoogenboom, R.; Schubert, U. S. A Fluorescent Thermometer Based on a Pyrene-Labeled Thermoresponsive Polymer. *Sensors* **2010**, *10* (9), 7979−7990.

(13) Dembska, A.; Juskowiak, B. Pyrene Functionalized Molecular Beacon with PH-Sensitive i-Motif in a Loop. *Spectrochim. Acta, Part A* **2015**, *150*, 928−933.

(14) Claucherty, S.; Sakaue, H. An Optical-Chemical Sensor Using Pyrene-Sulfonic Acid for Unsteady Surface Pressure Measurements. *Sens. Actuators, A* **2021**, *317*, 112359.

(15) Rossi, N. A. A.; Duplock, E. J.; Meegan, J.; Roberts, D. R. T.; Murphy, J. J.; Patel, M.; Holder, S. J. Synthesis and Characterisation of Pyrene -Labelled Polydimethylsiloxane Networks: Towards the in Situ Detection of Strain in Silicone Elastomers. *J. Mater. Chem.* **2009**, *19* (41), 7674−7686.

(16) Roberts, D. R. T.; Patel, M.; Murphy, J. J.; Holder, S. J. Optical Response to Stress in Pyrene Labelled Polydimethylsiloxane Elastomers: Monitoring Strain in 1D and 2D. *Sens. Actuators, B* **2012**, *162* (1), 43−56.

(17) Cellini, F.; Block, L.; Li, J.; Khapli, S.; Peterson, S. D.; Porfiri, M. Mechanochromic Response of Pyrene Functionalized Nanocomposite Hydrogels. *Sens. Actuators, B* **2016**, *234*, 510−520.

(18) Kovalev, I. S.; Taniya, O. S.; Slovesnova, N. V.; Kim, G. A.; Santra, S.; Zyryanov, G. V.; Kopchuk, D. S.; Majee, A.; Charushin, V. N.; Chupakhin, O. N. Fluorescent Detection of 2,4-DNT and 2,4,6-TNT in Aqueous Media by Using Simple Water-Soluble Pyrene Derivatives. *Chem. - Asian J.* **2016**, *11* (5), 775−781.

(19) Bains, G.; Patel, A. B.; Narayanaswami, V. Pyrene: A Probe to Study Protein Conformation and Conformational Changes. *Molecules* **2011**, *16* (9), 7909−7935.

(20) Somerharju, P. Pyrene-Labeled Lipids as Tools in Membrane Biophysics and Cell Biology. *Chem. Phys. Lipids* **2002**, *116* (1), 57−74.

(21) Krasheninina, O. A.; Novopashina, D. S.; Apartsin, E. K.; Venyaminova, A. G. Recent Advances in Nucleic Acid Targeting Probes and Supramolecular Constructs Based on Pyrene-Modified Oligonucleotides. *Molecules* **2017**, *22* (12), 2108.

(22) Winnik, F. M. Photophysics of Preassociated Pyrenes in Aqueous Polymer Solutions and in Other Organized Media. *Chem. Rev.* **1993**, *93* (2), 587−614.

(23) Karuppannan, S.; Chambron, J.-C. Supramolecular Chemical Sensors Based on Pyrene Monomer−Excimer Dual Luminescence. *Chem. - Asian J.* **2011**, *6* (4), 964−984.

(24) Weinstain, R.; Slanina, T.; Kand, D.; Klán, P. Visible-to-NIR-Light Activated Release: From Small Molecules to Nanomaterials. *Chem. Rev.* **2020**, *120* (24), 13135−13272.

(25) Jiang, J.; Tong, X.; Zhao, Y. A New Design for Light-Breakable Polymer Micelles. *J. Am. Chem. Soc.* **2005**, *127* (23), 8290−8291.

(26) Moad, G.; Chiefari, J.; Chong, Y. K.; Krstina, J.; Mayadunne, R. T. A.; Postma, A.; Rizzardo, E.; Thang, S. H. Living Free Radical Polymerization with Reversible Addition − Fragmentation Chain Transfer (the Life of RAFT). *Polym. Int.* **2000**, *49* (9), 993−1001.

(27) Keddie, D. J.; Moad, G.; Rizzardo, E.; Thang, S. H. RAFT Agent Design and Synthesis. *Macromolecules* **2012**, *45* (13), 5321−5342.

(28) Morpurgo, M.; Veronese, F. M.; Kachensky, D.; Harris, J. M. Preparation and Characterization of Poly(Ethylene Glycol) Vinyl Sulfone. *Bioconjugate Chem.* **1996**, *7* (3), 363−368.

(29) Lutolf, M. P.; Hubbell, J. A. Synthesis and Physicochemical Characterization of End-Linked Poly(Ethylene Glycol)-Co-Peptide Hydrogels Formed by Michael-Type Addition. *Biomacromolecules* **2003**, *4* (3), 713−722.

(30) Rehmann, M. S.; Skeens, K. M.; Kharkar, P. M.; Ford, E. M.; Maverakis, E.; Lee, K. H.; Kloxin, A. M. Tuning and Predicting Mesh Size and Protein Release from Step Growth Hydrogels. *Biomacromolecules* **2017**, *18* (10), 3131−3142.

(31) Wang, J.; Zhang, F.; Tsang, W. P.; Wan, C.; Wu, C. Fabrication of Injectable High Strength Hydrogel Based on 4-Arm Star PEG for Cartilage Tissue Engineering. *Biomaterials* **2017**, *120*, 11−21.

(32) Licht, C.; Rose, J. C.; Anarkoli, A. O.; Blondel, D.; Roccio, M.; Haraszti, T.; Gehlen, D. B.; Hubbell, J. A.; Lutolf, M. P.; De Laporte, L. Synthetic 3D PEG-Anisogel Tailored with Fibronectin Fragments

Induce Aligned Nerve Extension. *Biomacromolecules* **2019**, *20* (11), 4075−4087.

(33) You, J.; Yoon, J. A.; Kim, J.; Huang, C.-F.; Matyjaszewski, K.; Kim, E. Excimer Emission from Self-Assembly of Fluorescent Diblock Copolymer Prepared by Atom Transfer Radical Polymerization. *Chem. Mater.* **2010**, *22* (15), 4426−4434.

(34) Riener, C. K.; Kada, G.; Gruber, H. J. Quick Measurement of Protein Sulfhydryls with Ellman's Reagent and with 4,4′-Dithiodipyridine. *Anal. Bioanal. Chem.* **2002**, *373* (4), 266−276.

(35) Ohnsorg, M. L.; Ting, J. M.; Jones, S. D.; Jung, S.; Bates, F. S.; Reineke, T. M. Tuning PNIPAm Self-Assembly and Thermoresponse: Roles of Hydrophobic End-Groups and Hydrophilic Comonomer. *Polym. Chem.* **2019**, *10* (25), 3469−3479.

(36) Birks, J. B. Excimers and Exciplexes. *Nature* **1967**, *214* (5094), 1187−1190.

(37) Iwamura, M.; Ishikawa, T.; Koyama, Y.; Sakuma, K.; Iwamura, H. 1-Pyrenylmethyl Esters, Photolabile Protecting Groups for Carboxylic Acids. *Tetrahedron Lett.* **1987**, *28* (6), 679−682.

(38) Hamasaki, A.; Sato, N.; Kubo, K.; Katsuki, A.; Ozeki, S. Switching of Fluorescence Wavelength Caused by Phase Separation of Pyrene in Poly(N-Isopropylacrylamide) Gel. *Chem. Lett.* **2019**, *48* (8), 902−905.

(39) Hong, Y.; Lam, J. W. Y.; Tang, B. Z. Aggregation-Induced Emission: Phenomenon, Mechanism and Applications. *Chem. Commun.* **2009**, No. 29, 4332−4353.